Copyright © 2010 Tech Science Press CMES, vol.64, no.3, pp.251-266, 2010

A Numerical Study of the Influence of Surface Roughness on the Convective Heat Transfer in a Gas Flow

F. Dierich[1] **and P.A. Nikrityuk**[1]

Abstract: This work presents a numerical investigation of the influence of the roughness of a cylindrical particle on the drag coefficient and the Nusselt number at low Reynolds numbers up to 40. The heated cylindrical particle is placed horizontally in a uniform flow. Immersed boundary method (IBM) with a continuous forcing on a fixed Cartesian grid is used. The governing equations are the Navier Stokes equation and the conservation of energy. A finite-volume based discretization and the SIMPLE algorithm with collocated-variables and Rie-Chow stabilization were used to solve the set of equations. Numerical simulations showed that the impact of the roughness on the drag coefficient is low. But we found out that the roughness has significant impact on the surface averaged Nusselt number. In particular, the Nusselt number decreases rapidly with increase of the roughness thickness. Based on the numerous simulations a mathematical dependency of the heat transfer efficiency factor on the surface ratio was obtained.

Keywords: Convective heat transfer, Roughness, Immersed boundary method

1 Introduction

Flow past a circular cylinder is a well accepted *'benchmark'* tool to study the drag forces and heat transfer in bluff body wakes, e.g. see Schlichting and Gersten (2006). The extensive review of numerical investigations of the flow dynamics past a cylinder (done in early 1980s) can be found in Braza et al. (1986). It is a well known fact that at Reynolds numbers, $1 < Re < 46$, the flow past a cylinder is laminar, where a steady recirculation region with toroidal vortex occurs behind the cylinder. The size of the recirculation region growths with increasing Reynolds number. Here the Reynolds number is defined as $Re = U_0 d/\nu$, where U_0 is the free-stream velocity, d is the diameter of cylinder, and ν is the kinematic viscosity. At

[1] CIC Virtucon, Institut of Process- and Chemical Engineering, TU Bergakademie Freiberg, Reiche Zeche/Fuchsmuelenweg 9, 09599 Freiberg, Germany. E-mails: Frank.Dierich@vtc.tu-freiberg.de, Petr.Nikrityuk@vtc.tu-freiberg.de

Reynolds numbers $Re \geq 46$, the flow becomes unsteady with vortex shedding (von Karman vortex shedding) in the near wake behind the cylinder. Many simulations were done to study the role of convection on the heat transfer near the cylinder, e.g. see Juncu (2004), including the influence of a porous layer around the cylinder on the enhancement of the heat transfer, see the work done by Bhattacharyya and Singh (2009). Bhattacharyya and Singh (2009) showed that a thin porous wrapper made of the same thermal conductivity as the cylinder can significantly reduce the heat transfer. To model the gas flow inside the porous layer they used the Dupuit-Forchheimer relationship, which states that the velocity inside the porous media is proportional to the bulk velocity multiplied by the porosity. The use of this assumption or the Darcy law assumption for the modeling of particle roughness is questionable due to the fact that the convection may not be negligible within the roughness region. An alternative way to explore the influence of a roughness on the heat transfer near the solid body is the direct modeling of a rough surface by use of Immersed Boundary Method (IBM), see Peskin (1972); Mittal and Iaccarino (2005); da Silva et al. (2009).

In the present work we use IBM in continuous forcing mode, for details see the classification done by Mittal and Iaccarino (2005). The main objective of this paper is the investigation of the flow and heat transfer from a rough solid cylinder placed horizontally in a cross-flow due to a uniform stream of air with a Prandtl number of 0.5. The cylinder is assumed to be heated with a uniform surface temperature. The temperature difference between the free stream flow and the surface of the cylinder is equal to 20 K. We consider the roughness layer to be made from the same material as the cylinder. Thus, the main motivation of this study is to estimate the influence of the thickness of roughness layer on the heat transfer and on the drag coefficient for a cylindrical particle.The practical context of this study is the understanding of the impact of particle roughness on the heat transfer in particulate flows. This kind of knowledge can be used by the enhancement of Nu-based heat transfer models by simulations of fixed- or fluidized bed systems.

2 Problem formulation and governing equations

We consider a single cylindrical particle with a diameter D_1 placed stationary, with the main gas flow passing around it. The inflow velocity, U_0, was assumed to be uniform and was determined by means of the Reynolds number calculated as follows:

$$Re = \frac{U_0 D_1}{\nu} \tag{1}$$

where ν is the kinematic viscosity.

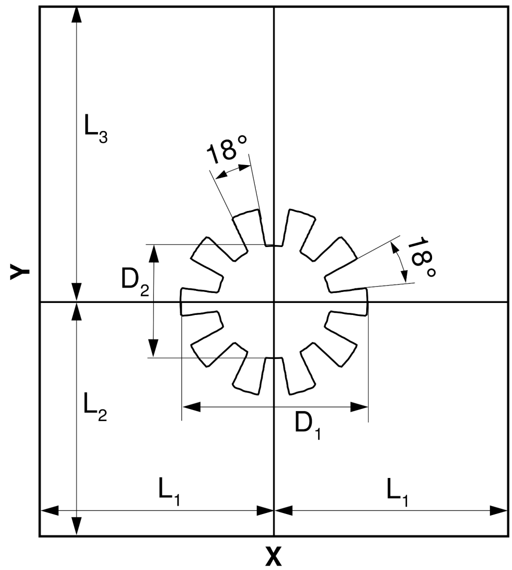

Figure 1: Principal scheme of the set up under investigation

The principal scheme of the domain is shown in Fig. 1. The rough particle consists of an inner cylinder with the diameter D_2 and an outer cylinder with 10 notches and the radius D_1 as shown in Figure 1. It is placed in the center of the domain with $L_1 = 20D_1$, $L_2 = 20D_1$ and $L_3 = 50D_1$. The diameter D_2 is varied from $0.5D_1$ to $1D_1$ to simulate different roughness. To proceed with the governing equations the following basic assumptions have been done:

1. The gas flow is treated as incompressible media.
2. The viscous heating effect is neglected.
3. The thermophysical properties are constant giving the Prandtl number, *Pr*, of about 0.5.
4. The buoyancy effect is neglected.

Taking into account the assumptions done above the conservation equations for mass-, momentum and energy transport written for the gas phase have the following form:

$$\nabla \cdot \vec{u} = 0, \tag{2}$$

$$\frac{\partial \vec{u}}{\partial t} + (\vec{u}\cdot\nabla)\,\vec{u} = -\frac{\nabla p}{\rho} + \nu\nabla^2\vec{u} - \nu\frac{\vec{u}}{K_u} + \vec{g}\,\beta_T\,(T - T_{ref})\,, \tag{3}$$

$$\frac{\partial T}{\partial t} + (\vec{u}\cdot\nabla)\,T = \frac{\lambda}{\rho c_p}\nabla^2 T - \frac{1}{\rho c_p}\frac{(T - T_s)}{K_T}. \tag{4}$$

Here $\vec{u}$ is the velocity vector, p is the pressure, ν is the kinematic viscosity, λ is the thermal conductivity, ρ is the density, c_p is the heat capacity, T_s is the temperature of the particle, β_T is the thermal expansion coefficient, T_{ref} is the reference temperature. It should be noted that in spite of the neglecting of the buoyancy effect the last term is included due to the validation case.

On the bottom we set an inflow boundary condition with constant temperature. We treat the top with an outlet boundary condition and on the sides we apply a symmetry boundary condition.

To set the no-slip and the thermal Dirichlet boundary conditions on the particle surface we tread the interface as porous with a permeability coefficient given by:

$$K_u = \frac{\varepsilon^3}{c_u\,(1-\varepsilon)^2}, \tag{5}$$

$$K_T = \frac{\varepsilon^3}{c_T\,(1-\varepsilon)^2}, \tag{6}$$

where ε is the volume fraction of gas, c_u and c_T are constants, which dimensions make K_u and K_T consistent with the units of the rest of the terms in the momentum and energy equations, respectively. The constants c_u and c_T are grid dependent and must be chosen manually. For example, if c_u takes too small value, the velocity inside the particle is not zero and the particle is treated as porous one. On the contrary, if c_u has too large value, the solution is not converging usually. Based on the numerous tests, in our case we found out that the choice:

$$c_u = 2\cdot 10^4\,\Delta x_{\min}^{-1} \tag{7}$$

$$c_T = 1\cdot 10^4\,\Delta x_{\min}^{-1} \tag{8}$$

with $\Delta x_{\min}^{-1}$ is the edge length of the smallest control volume inside the particle. In this work $\Delta x_{\min} \approx 7.3\cdot 10^{-3}\,D_1$.

The volume fraction of gas ε takes the following values:

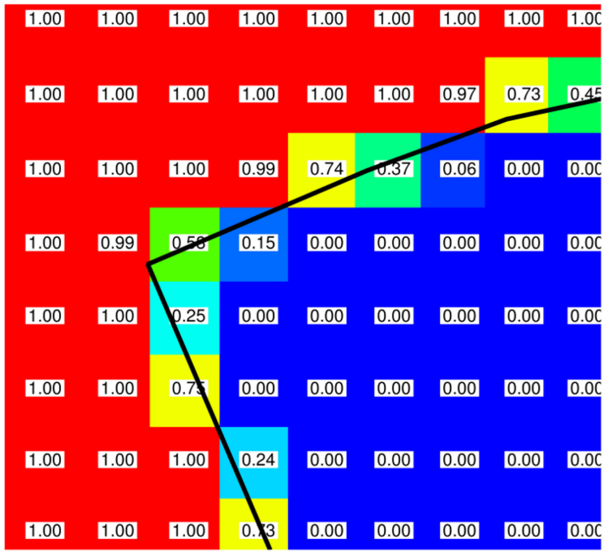

Figure 2: Zoomed view of the spatial distribution of the volume fraction of gas near the particle notch.

$$\varepsilon = \begin{cases} 1, & \text{for} \quad \text{the gas phase} \\ 0, & \text{for} \quad \text{the solid phase} \\ 0\ldots 1, & \text{for} \quad \text{the interface cells} \end{cases} \tag{9}$$

For calculating the volume fraction of gas in each control volume we use a two-step algorithm. The first step of this algorithm consists in the description of the particle by a polygon. The second step uses the Sutherland-Hodgman clipping algorithm, for details see I. E. Sutherland and G. W. Hodgman (1974), to calculate the volume fraction of gas based on a polygon intersection with the 'walls' of a control volume. Fig. 2 shows zoomed view of the spatial distribution of ε the particle interface.

3 Numerics and Validation

The set of transport equations has been discretized by a finite-volume, finite-difference based method. The SIMPLE algorithm with collocated-variables arrangement was used to calculate the pressure and the velocities, for details see Ferziger and Peric (2002). Rhie and Chow stabilization scheme was used for the stabilization of pressure-velocity coupling, see Rhie and Chow (1983).

To set up the 'internal' boundary conditions on the particle surface the source terms $-\nu\frac{\vec{u}}{K_u}$ and $-\frac{1}{\rho c_p}\frac{(T-T_s)}{K_T}$ in eqs. (3) and (4), respectively, are linearized following recommendations given by Patankar (1980) as follows:

$$S = S_C + S_P\phi_P^{bc} \tag{10}$$

where ϕ_P^{bc} is the value of principal variable (T_s or u_s) inside the solid region. Applied this equation in our case we have:

$$S_C^u = 0,\ S_P^u = -\nu\frac{1}{K_u} \qquad S_C^T = \frac{1}{\rho c_p}\frac{T_s}{K_T},\ S_P^T = -\frac{1}{\rho c_p}\frac{1}{K_T} \tag{11}$$

Here the term $\frac{1}{K}$ is nothing else then a number large enough to make the other terms in the discretization equation negligible in a such way that:

$$S_C + S_P T_P \approx 0, \qquad T_p = -\frac{S_C^T}{S_P^T} = T_s \tag{12}$$

Time marching with fixed time step was used. For every time step the outer iterations were stopped if the normalized maximal residual of all equations is less than 10^{-10} corresponding to 10 orders of magnitude. We used a grid with 400×600 control volumes. The size of a control volume (CV) inside the solid particle is about one hundredth of the particle diameter. This is achieved by local refinement of the grid inside the particle. The time step was equal to 0.1 sec, which is in non-dimensional time $6.25\cdot10^{-4}$. It should be noted that unsteady simulations were necessary in order to obtain the steady-state solution. Thus, all results presented in this work are related steady state regimes only. To validate the code and the model we reproduced the results of the flow around a cylinder at Reynolds number $Re = 20$. We compared the drag coefficient C_D, the angle of separation θ_s and the vortex length L/r, where r is the radius of the cylinder as shown in Figure 3. Table 1 shows that the present results are in good consistent with other data published.

Next, we validated our model and the code against experimental results of [Kuehn (1976); Kuehn and Goldstein (1978)]. The test case compares the numerical prediction of temperature profiles along the symmetry lines with experimental data. Experimental set up includes a heated inner cylinder placed in the center of another cold cylinder, see Fig. 4. Due to the gravity field a buoyancy-induced flow occurs. The inner cylinder with the radius of $R_i = 0.0178\,\mathrm{m}$ has the surface temperature

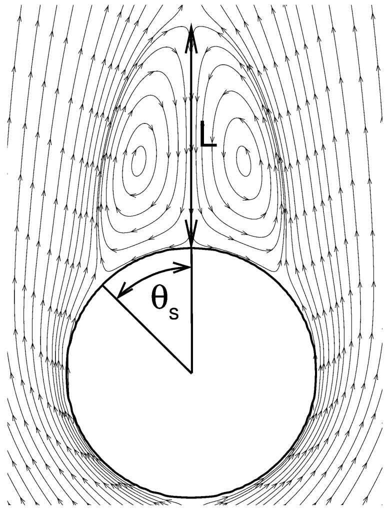

Figure 3: Definition of angel of separation (θ_s) and the vortex length (L)

Authors	C_D	θ_s	L/r
Juncu (2004)	1.99	43.24	1.79
Fornberg (1980)	2.000	45.3	1.82
He and Doolen (1997)	2.152	42.96	1.842
Present	1.99	43.9	1.86

Table 1: Validation I: fluid flow past a cylinder. The definition of parameters θ_s and L/r is given in Fig. 3.

$T_i = 373\,\mathrm{K}$ and the outer cylinder with the radius of $R_0 = 0.0463\,\mathrm{m}$ has the temperature $T_0 = 327\,\mathrm{K}$. The space between cylinders is filled with the air having the following transport properties:

$$\rho = 1.08\,\mathrm{kg\,m^{-3}},\ \beta_T = 2.83\cdot 10^{-3}\,\mathrm{K^{-1}},\ c_p = 1008\,\mathrm{J\,kg^{-1}\,K^{-1}}$$
$$\lambda = 0.02967\,\mathrm{W\,m^{-1}\,K^{-1}},\ \mu = 2.081\cdot 10^{-5}\,\mathrm{kg\,m^{-1}\,s^{-1}}. \tag{13}$$

The whole set-up corresponds to the following non-dimensional numbers:

$$Gr = \frac{g\,\beta_T\,(T_i - T_0)\,(R_0 - R_i)^3}{\nu^2} = 7.912 \cdot 10^4$$
$$Pr = \frac{c_p\,\mu}{\lambda} = 0.707 \tag{14}$$
$$Ra = Gr \cdot Pr = 5.594 \cdot 10^4$$

The numerical simulations were performed by use of two grids having 50×50 CV and 100×100 CV, respectively. The gas between cylinders was treated as incompressible media. Additional simulations done by use of a commercial software where the gas was taken as compressible media showed identical results. The temperature contour plot and the flow pattern are shown in Fig. 5. The comparison of temperature profiles along the symmetry line compared with the data of Kuehn (1976); Kuehn and Goldstein (1978) are given in Fig. 6. It can be seen that the agreement between our predictions and the experimental data is very good.

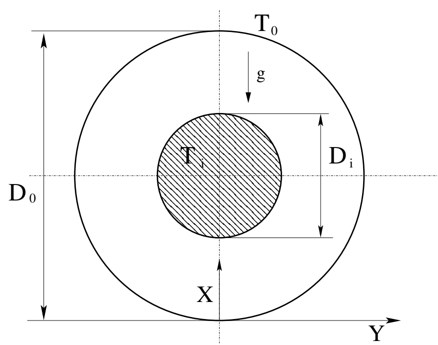

Figure 4: Validation II: Scheme of set-up.

4 Results

The present problem can be governed by four parameters: the Reynolds number *Re*, which is defined by eq. (1), the Nusselt number, the heat transfer efficiency factor E_f and the surface enlargement S_{ef}. On the surface of the cylinder, the local Nusselt number Nu_{local} can be defined and thus the surface–averaged Nusselt number Nu_{av} is given as:

$$Nu_{av} = \frac{\oint_S Nu_{local}\, ds}{\oint_S 1\, ds}, \qquad Nu_{local} = \frac{D_1}{T_s - T_\infty}\frac{\partial T}{\partial n} \tag{15}$$

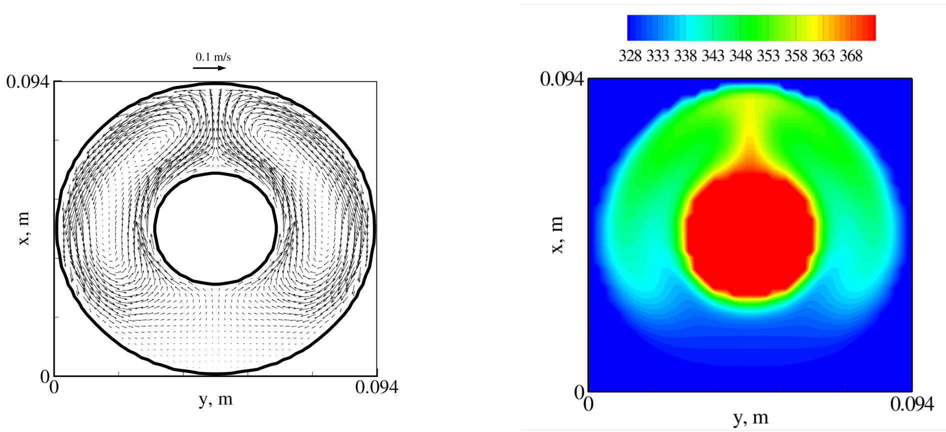

Figure 5: Validation II: The spatial distribution of the velocity vectors and contour plot of the temperature

where T_∞ is the free stream temperature, T_s is the particle surface temperature and n is the inward-pointing normal. In this work $T_s - T_\infty$ was set to 20 K, where $T_\infty =$ 300 K.

In order to study the influence of roughness on the heat transfer we introduce the heat transfer efficiency factor E_f, Bhattacharyya and Singh (2009), given by:

$$E_f = \frac{Nu_{av}}{Nu^0_{av}} \tag{16}$$

where Nu^0_{av} is the surface average Nusselt number for the particle with zero roughness. Thus, E_f measures the ratio between the average rate of heat transfer from a rough particle to the average rate of heat transfer from a particle without roughness. Thus, $E_f > 1$ corresponds to heat transfer enhancement and $E_f < 1$ corresponds to insulation.

The last parameter to characterize the roughness is the surface enlargement S_{ef} given by:

$$S_{ef} = \frac{S_{rough}}{S_0} \tag{17}$$

where S_0 and S_{rough} are the geometric surface area of the particle without roughness and with roughness, respectively.

The equation for the calculation of the drag coefficient have the following form:

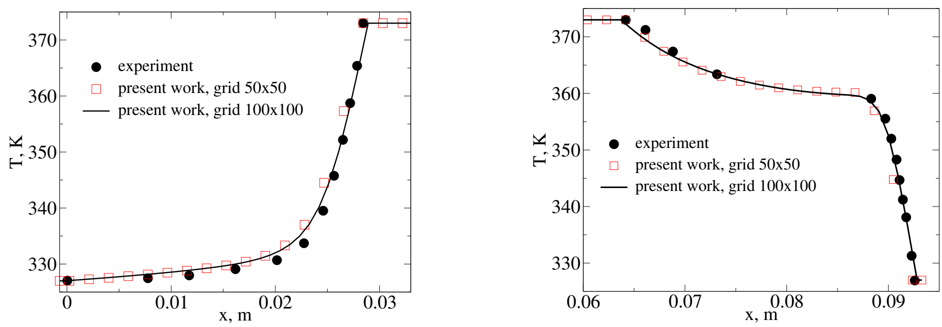

Figure 6: Validation II: The temperature profiles at the vertical symmetry line. Here the experimental data corresponds to the results of Kuehn (1976); Kuehn and Goldstein (1978)

S_{ef}	D_2/D_1	Re = 10	Re = 20	Re = 40
1.00	1.00	2.76	1.99	1.50
1.13	0.95	2.81	2.03	1.53
1.27	0.90	2.85	2.07	1.56
2.07	0.60	2.93	2.14	1.62

Table 2: Drag coefficient (C_D) in different Re and S_{ef}

$$C_D = \frac{F_D}{\frac{1}{2}\rho U_0^2 D_1} \qquad \vec{F} = \oint \left(-p\vec{n} + \nu\left(\nabla\vec{u} + \nabla\vec{u}^T\right)\cdot\vec{n}\right) ds \tag{18}$$

The vector $\vec{F}$ is the hydrodynamic force acting on the particle. In this work the drag force F_D corresponds to F_y, see Fig. 1.

The numerical simulations were done for three Reynolds numbers 10, 20 and 40. By fixing the Reynolds number we investigate systematically the influence of the roughness of the cylinder on the surface averaged Nusselt number. The roughness of the particle was increased by the decrease of the diameter D_2, see Fig. 1.

Fig. 7a shows an example of the velocity distribution near the particle surface for Re = 40 and $D_2/D_1 = 0.6$. It can be seen that the velocity is zero in the dimples. Thus, the air in the dimples plays the role of an isolator, which decreases the convective heat transfer. This effect can be clearly seen in the Fig. 7b, which depicts the temperature profiles along the symmetry line for different Re numbers. Our results show that due to the 'isolation' effect produced by the dimples, the temperature

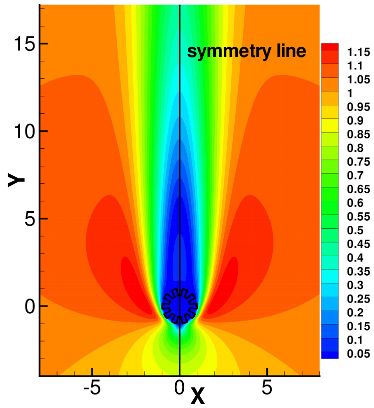

a

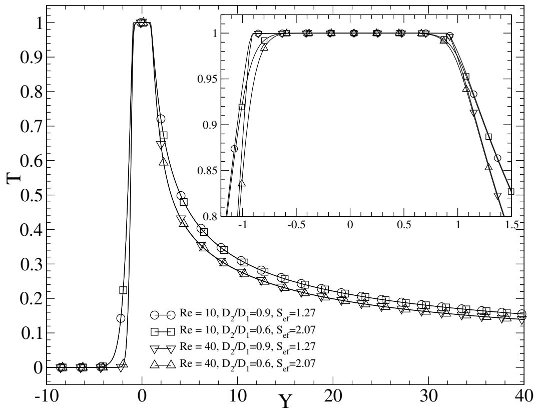

b

Figure 7: Contour plot of non-dimensional velocity magnitude $\frac{\sqrt{u_x^2+u_y^2}}{u_{in}}$ with Re = 40 and $D_2/D_1 = 0.6$, $S_{ef} = 2.07$ - a, Non-dimensional temperature profiles $\frac{T-T_\infty}{T_s-T_\infty}$ along the symmetry line for different Reynolds numbers - b.

profiles near the interface are not so steep in comparison to the cases with less roughness. Thus, the temperature gradient in the dimples is decreased. But at the same time we have the increase of the temperature gradient in front of the convex ledge on the particle surface. This can be seen in the Fig. 8, which shows contour plots of the non-dimensional temperature gradient $\frac{D_1}{\Delta T}\sqrt{(\partial_x T)^2+(\partial_y T)^2}$. It can be seen that the local heat transfer changes dramatically. In particular, we have temperature gradients concentrated on the particle ledges. This effect can play a very import role at the combustion of rough particles leading to the local speed-up of heterogeneous chemical reactions on the convex shaped interfaces.

Next, we show the contour plots of the non-dimensional temperature, see Fig. 9. The increase of the Re number at a constant value of S_{ef} leads to the decrease of the thermal boundary layer, which is well know fact. But at the same time the increase of the surface enlargement at a constant value of Re leads to the increase of the thickness of the effective thermal boundary layer and as a result, the surface averaged Nusselt number decreases with the increase of S_{ef}. This effect can be seen in Fig. 10. It can be seen that the efficiency factor E_f is proportional to the surface enlargement coefficient S_{ef} as follows $E_f = S_{ef}^{-\frac{5}{4}}$.

In comparison to the behavior of the Nusselt number, the drag coefficient C_D increases insignificantly with the increase of the roughness, see Tab. 2. We explain

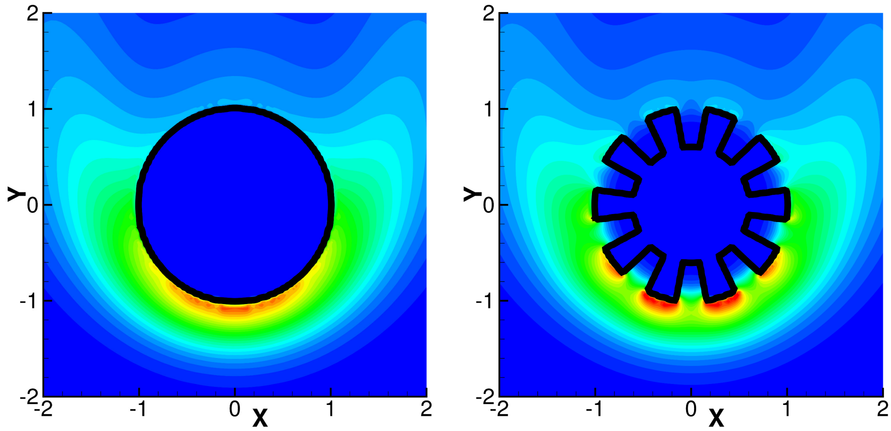

Figure 8: Contour plots of the non-dimension temperature gradient $\frac{D_1}{\Delta T}\sqrt{(\partial_x T)^2 + (\partial_y T)^2}$. Here the maximum in the left figure is 5.2 and the maximum in the right figure is 5.86, the minimum is 0.

this effect by insignificant influence of the roughness on the hydrodynamic boundary layer. To demonstrate it Fig. 11 plots the azimuthal profile of the velocity magnitude at the distance of $0.1D_1$ from D_1. It can be seen that profiles calculated for the rough and smooth particles are almost identical excepting the region at $\theta = \pm 135°$.

5 Conclusions

A numerical investigation of steady laminar flow past a heated cylindrical particle with different roughness was carried out. The effect of the thickness of the roughness layer on the flow and heat transfer were systematically investigated. Based on the presented numerical data and discussions several conclusions can be summarized as follows:

1. The roughness has significant impact on the surface averaged Nusselt number. In particular, the Nusselt number decreases rapidly with increase of the roughness thickness.

2. The efficiency factor E_f is proportional to the surface enlargement coefficient S_{ef} as follows $E_f = S_{ef}^{-\frac{5}{4}}$

3. The impact of the roughness on the drag coefficient is low.

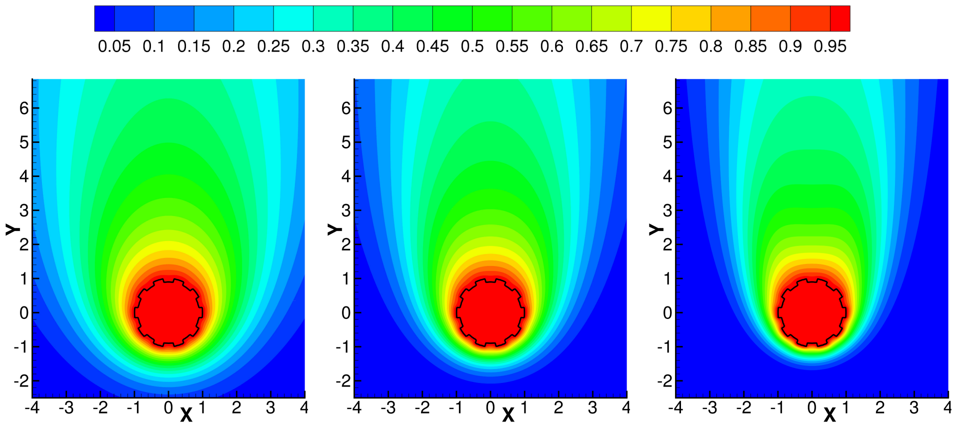

(a) Re = 10, $D_2/D_1 = 0.9$, $S_{ef} = 1.27$ (b) Re = 20, $D_2/D_1 = 0.9$, $S_{ef} = 1.27$ (c) Re = 40, $D_2/D_1 = 0.9$, $S_{ef} = 1.27$

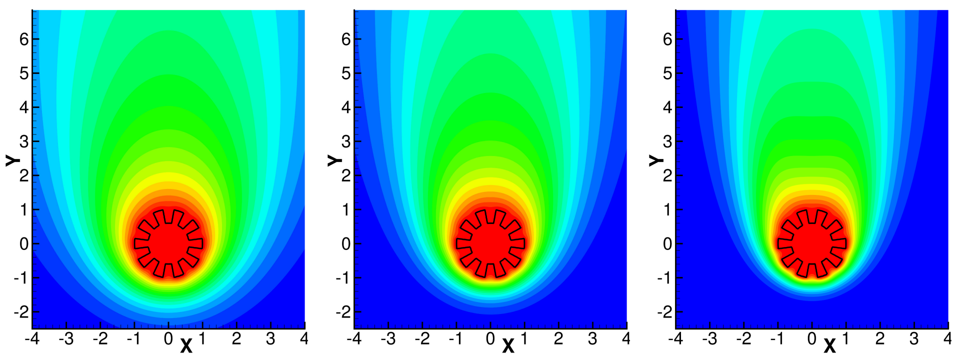

(d) Re = 10, $D_2/D_1 = 0.6$, $S_{ef} = 2.07$ (e) Re = 20, $D_2/D_1 = 0.6$, $S_{ef} = 2.07$ (f) Re = 40, $D_2/D_1 = 0.6$, $S_{ef} = 2.07$

Figure 9: Contour plots of the non-dimensional temperature $\frac{T-T_\infty}{T_s-T_\infty}$ in different Reynolds numbers Re and roughnesses.

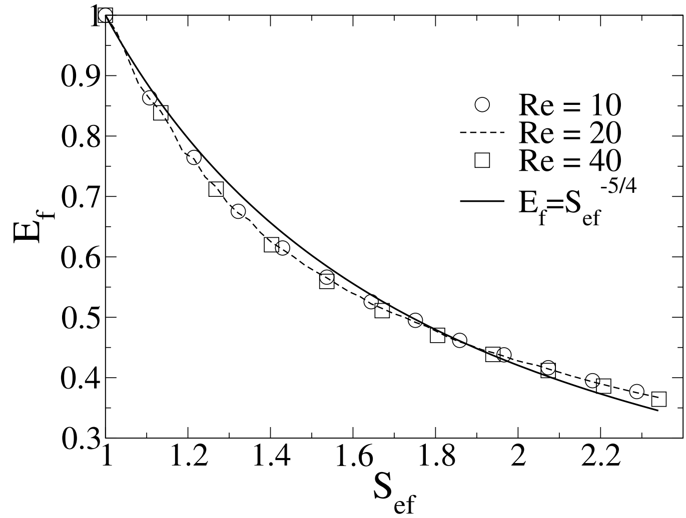

Figure 10: Effect of surface enlargement(S_{ef}) on the efficiency factor (E_f)

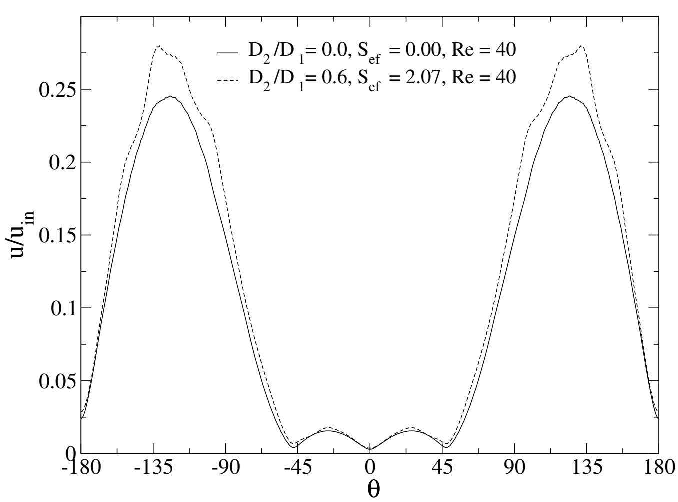

Figure 11: Azimuthal profile of the velocity magnitude at the distance of $0.1D_1$ from the D_1.

Acknowledgement: This work was financially supported by the Government of Saxony and the Federal Ministry of Education and Science of Federal Republic of Germany as a part of CIC VIRTUHCON. The administration of TUBAF is gratefully acknowledged for the support. We thank anonymous reviewer for very helpful comments.

References

Schlichting, H.; Gersten, K. (2006): *Grenzschicht-Theorie*. Springer. 10nd Edition.

Fornberg, B. (1980): A numerical study of steady viscous flow past a circular cylinder. *J. Fluid Mech.*, vol. 4, pp. 819–855.

Braza M.; Chassaing P.; Minh Ha. (1986): Numerical study and physical analysis of the pressure and velocity fields in thenear wake of a circular cilinder. *J. Fluid Mechanics*, vol. 165, pp. 79-130.

He, X.; Doolen, G. (1997): Lattice Boltzmann Method on Curvilinear Coordinates System: Flow around a Circular Cylinder. *J. Comput. Phys.*, vol. 134, pp. 306–315.

Juncu, Gh. (2004): Unsteady conjugate heat/mass transfer from a circular cylinder in laminar crossflow at low Reynolds numbers. *Int. J. Heat Mass Transfer*, vol. 47, pp. 2469–2480.

Bhattacharyya, S.; Singh, A.K. (2009): Augmentation of heat transfer from a solid cylinder wrapped with a porous layer. *Int. J. Heat Mass Transfer*, vol. 52, pp. 1991–2001.

Peskin C.S. (1972): Flow pattern around heart valves: a numerical method. *J. Comput. Phys.*, vol. 10, pp. 252–271.

Mittal, R.; Iaccarino, G. (2005): Immersed boundary methods. *Annu. Rev. Fluid Mech.*, vol. 37, pp. 239–261.

da Silva, A.R.; Silveira-Neto, A.; Rade, D.A.; Francis, R.; Santos, E.A. (2009): Numerical simulations of flows over a pair of cylinders at different arrangements using the immersed boundary method. *CMES: Computer Modeling Eng. & Sci.*, vol. 50, pp. 285–303.

Sutherland, I.E.; Hodgman, G.W. (1974): Reentrant Polygon Clipping. *Communications of the ACM (CACM)*, vol. 17, pp. 32–42.

S.V. Patankar (1980): *Numerical Heat Transfer and Fluid Flow*. Hemisphere Publishing Corporation.

J. Ferziger; M. Peric (2002): *Computational Methods for Fluid Dynamics*. Springer. 3nd Edition.

C.M. Rhie; W.L. Chow (1983): Numerical study of the turbulent flow past an airfoil with trailing edge separation. *AIAA*, vol. 21, pp. 1525–1532.

Kuehn, T.H.; Goldstein, R.J. (1978): An experimental study of natural convection heat transfer in concentric and eccentric horizontal cylindrical annuli. *Journal of Heat Transfer*, vol. 100, pp. 635–640.

Kuehn, T.H.; Goldstein, R.J. (1976): An experimental and theoretical study of natural convection in the annulus between horizontal concentric cylinders. *J. Fluid Mech.*, vol. 74, pp. 695–719.

Khadra, K.; Angot, P.; Parneix, S.; Caltagirone, J.P. (2000): Fictitious domain approach for numerical modelling of Navier-Stokes equations. *Int. J. Numer. Methods Fluids.*, vol. 34, pp. 651–684.